

Iterative removal of sources to model the turbulent electromotive force

Abhijit B. Bendre^{1,5*}, Jennifer Schober¹, Prasun Dhang^{2,4} and Kandaswamy Subramanian^{2,3}

¹*Institute of Physics, Laboratory of Astrophysics, École Polytechnique Fédérale de Lausanne (EPFL), 1290 Sauverny, Switzerland*

²*IUCAA, Post Bag 4, Ganeshkhind, Pune 411007, India*

³*Department of Physics, Ashoka University, Rajiv Gandhi Education City, Rai, Sonapat 131029, Haryana, INDIA*

⁴*JILA, University of Colorado and National Institute of Standards and Technology, 440 UCB, Boulder, CO 80309-0440, USA*

⁵*Scuola Normale Superiore di Pisa, Piazza dei Cavalieri 7, 56126 Pisa, Italy*

Accepted XXX. Received YYY; in original form ZZZ

ABSTRACT

We describe a novel method to compute the components of dynamo tensors from direct magnetohydrodynamic (MHD) simulations. Our method relies upon an extension and generalisation of the standard Högbom CLEAN algorithm widely used in radio astronomy to systematically remove the impact of the strongest beams onto the corresponding image. This generalisation, called the Iterative Removal of Sources (IROS) method, has been adopted here to model the turbulent electromotive force (EMF) in terms of the mean magnetic fields and currents. Analogous to the CLEAN algorithm, IROS treats the time series of the mean magnetic field and current as beams that convolve with the dynamo coefficients which are treated as (clean) images to produce the EMF time series (the dirty image). We apply this method to MHD simulations of galactic dynamos, to which we have previously employed other methods of computing dynamo coefficients such as the test-field method, the regression method, as well as local and non-local versions of the singular value decomposition (SVD) method. We show that our new method reliably recovers the dynamo coefficients from the MHD simulations. It also allows priors on the dynamo coefficients to be incorporated easily during the inversion, unlike in earlier methods. Moreover, using synthetic data, we demonstrate that it may serve as a viable post-processing tool in determining the dynamo coefficients, even when the power of additive noise to the EMF is twice as much as the actual EMF.

Key words: galaxies: magnetic fields – dynamo – ISM: magnetic fields – Magnetohydrodynamics (MHD) – methods: data analysis – turbulence

1 INTRODUCTION

Magnetic fields with long-range regularity are present in various astrophysical systems from stars to galaxies. Observational and numerical evidence suggests that the most plausible mechanism for their generation is the large-scale dynamo mechanism (Moffatt 1978; Beck & Wielebinski 2013; Rüdiger & Hollerbach 2004; Brandenburg & Subramanian 2005; Shukurov & Subramanian 2021). In this process, the magnetic field with scales of regularity much larger than the scale at which turbulence is driven, is generated at the expense of kinetic energy, with the aid of both large-scale shear and helical turbulence. This mechanism can be characterised in terms of mean-field electrodynamics (Krause & Raedler 1980), by first expressing the dynamical variables, velocity \mathbf{U} and magnetic field \mathbf{B} , as the sums of their respective mean or large-scale components ($\overline{\mathbf{U}}$ and $\overline{\mathbf{B}}$) and the fluctuating (or the small-scale) components (\mathbf{u} and \mathbf{b}). The mean is defined as an average over a suitable domain for which the Reynolds's averaging rules are satisfied. Which is to say that; $\overline{\partial \mathbf{B} / \partial t} = \partial \overline{\mathbf{B}} / \partial t$, $\overline{\partial \mathbf{B} / \partial x_i} = \partial \overline{\mathbf{B}} / \partial x_i$, $\overline{\mathbf{B}_1 + \mathbf{B}_2} = \overline{\mathbf{B}_1} + \overline{\mathbf{B}_2}$, $\overline{\mathbf{B}} = \overline{\mathbf{B}}$, $\overline{B_i b_j} = 0$, $\overline{B_i B_j} = \overline{B_i} \overline{B_j}$. The evolution of the mean magnetic field then depends on the mean velocity and turbulent EMF, i.e. the cross correlation between \mathbf{u} and \mathbf{b} , $\overline{\mathcal{E}_i} = \overline{(\mathbf{u} \times \mathbf{b})_i}$. This EMF is then

expressed in terms of the mean magnetic field itself and the system is closed, i.e.

$$\overline{\mathcal{E}_i} = \alpha_{ij} \overline{B_j} - \eta_{ij} (\nabla \times \overline{\mathbf{B}})_j, \quad (1)$$

when mean fields are defined using horizontal averaging¹ (see Eq. 2). Here α_{ij} and η_{ij} are the coefficients of the dynamo tensors, which in general relate to the statistical properties of the background turbulence. In the high conductivity limit, these coefficients are proportional to the specific turbulence properties such as the fluctuating kinetic and magnetic energy densities and their helicity densities. Therefore in the context of various astrophysical systems, these dynamo coefficients dictate how statistical properties of the background turbulence impact the evolution of large-scale magnetic fields. Observational estimates of the dynamo coefficients often rely upon assumptions and phenomenological properties of the turbulence. In the context of galactic dynamo, e.g., the estimation relies upon the observables such as correlation length scales of turbulence and the supernova (SN) rate (Krause & Raedler 1980; Shukurov & Subramanian 2021). Equally, analytical estimates of the transport coefficients (e.g. Cattaneo & Hughes 1996) make simplifying assumptions (such as isotropy of turbulence and high conductivity etc.) that are often

¹ We also note that we have used a convention such that the repeated indices are summed over.

* E-mail: abhijit.bendre@sns.it

questionable. Therefore direct magnetohydrodynamic (MHD) simulations of such systems with realistic turbulence driving and wherein the \mathbf{E} and \mathbf{B} are self-consistently generated, provide a very useful tool in estimating the dynamo coefficients.

Various methods to compute these dynamo coefficients from direct numerical simulations (DNS) have so far been suggested and tested. The plethora of methods reflects the fact that Eq. 1 represents an under-determined system and one that is not straightforward to invert. For example, Cattaneo & Hughes (1996) used the random magnetic field generated in helically driven turbulence with uniform imposed mean field to calculate the EMF and fit it against the imposed $\bar{\mathbf{B}}$ to compute the α_{ij} coefficients, while in Tobias & Cattaneo (2013) the authors used a method of determining the conductivity of solids from material science to determine the magnetic diffusivity. In a slightly different setup Park et al. (2023) explored the scenario of magnetically forced turbulence (with explicit helical magnetic forcing), and computed turbulent diffusivity using a semi-analytical approach. This is relevant for magnetic field amplification in magnetically dominated systems such as accretion disks, stellar coronas etc. In Brandenburg & Sokoloff (2002) and Kowal et al. (2006), the authors developed an approach to computing the dynamo coefficients by fitting the various moments of the EMF and mean fields against their respective linear relations. This method is designed to handle the additive noise in the EMF and mean magnetic field data assuming that they are uncorrelated. A method with similar capability and an additional advantage of quantifying the auto-correlations between the dynamo coefficients, uses singular value decomposition (SVD), and was applied to several contexts. These include the stellar dynamo simulations in Racine et al. (2011) and Simard et al. (2016), the interstellar medium (ISM) simulations in Bendre et al. (2020), and the global accretion disc simulations in Dhang et al. (2020). The same method was extended to explore the non-local dependence of EMF on mean magnetic fields in Bendre & Subramanian (2022) and to compute the scale-dependent dynamo coefficients in the ISM simulations.

As a more direct approach to invert Eq. 1, the kinematic test-field method was introduced by (Schirmer et al. 2005, 2007). In this method the additional test magnetic fields $\bar{\mathbf{B}}_T$ are passively evolved along with the DNS such that they do not affect the turbulent velocity $\bar{\mathbf{u}}$. The fluctuations (\mathbf{b}_T) generated through tangling of the test-fields by the turbulence, are recorded to further compute the additional EMF components, and so also the dynamo coefficients. The test-field method has an advantage of determining the dynamo coefficients at the length scale of imposed the test-fields, and it has been used in several different contexts, including helically driven turbulence, ISM turbulence, accretion disc turbulence, and even in the simulations of solar and geo-dynamos (Brandenburg 2005; Sur et al. 2007; Gressel et al. 2008; Käpylä et al. 2009; Bendre et al. 2015; Gressel & Pessah 2015; Warnecke et al. 2016). However, it often proves to be computationally expensive as it relies upon integrating the additional induction equations (associated with each test-field component) along with the rest of the MHD equations. Pros and cons of these methods have also been discussed in the literature (Brandenburg 2009, 2018; Shukurov & Subramanian 2021).

In this paper we introduce a novel method to determine the dynamo coefficients which is based on post-processing the data from turbulent dynamo DNS. For this we adopt a version of a deconvolution algorithm based on the Högbom CLEAN method (Högbom 1974) called IROS (Iterative Removal Of Sources) (Hammersley et al. 1992) to mitigate some of the issues in previous methods. This method is then tested against mock data and also applied to determine dynamo coefficients from a DNS of ISM simulations, for which comparison can

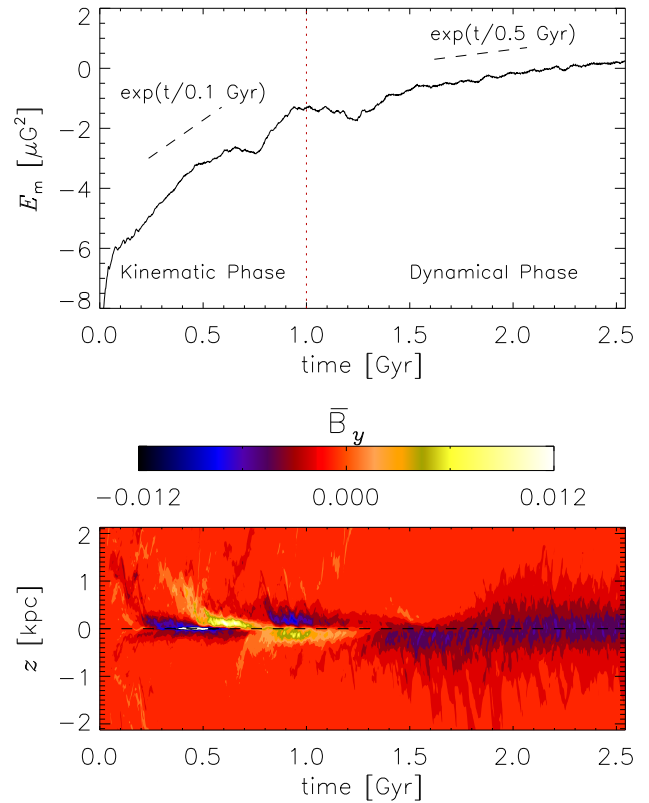


Figure 1. In the top panel, time evolution of the mean magnetic energy is shown and kinematic and the dynamical phases of magnetic field evolution are separated by a vertical red dotted line. In the bottom panel time evolution of the vertical profile of mean magnetic field (y -component) is shown. Colour-code is normalised with a factor of $\exp(-t/0.2 \text{ Gyr})$ in the kinematic phase and with $\exp(-t/1.0 \text{ Gyr})$ in the dynamical phase to compensate for the exponential amplification.

be made to the results from several of the other methods. We have also successfully applied this method to compute the dynamo coefficients for other systems as well (eg. Dhang et al. 2023; Qazi et al. 2024), where the turbulence itself is driven by magnetic instabilities. In Section 4, we apply the aforementioned methods to the mock data of EMF with an additive random noise. Further in Section 5 we apply these methods to the data of ISM simulations, which is followed by Section 6, where we discuss the conclusions.

This paper is structured as follows. In Section 2 we describe briefly the details of the ISM simulations, and the data which we use in the later sections to apply the IROS method. In Section 3.1 we describe the local version of the IROS method. It is followed by Section 3.2, where we explore the possibility of imposing physical constraints on the dynamo coefficients in the framework of IROS. In this analysis, we impose the constraints of symmetry or antisymmetry on the vertical profiles of these dynamo coefficients. Further in Section 5 we apply these methods to the data of ISM simulations, which is followed by Section 6, where we discuss the conclusions. The paper also has two appendices in which we describe respectively the application of IROS method to invert the non-local representation of EMF (Appendix A), and the one in which we represent the IROS method as a flowchart (Appendix B).

2 SIMULATIONS

As a test case for our new method of determining dynamo coefficients from DNS, we use the data from the direct MHD simulations of a fraction of a disc galaxy. Details of these simulation setups and their outcomes are described in [Bendre et al. \(2015\)](#) and [Bendre \(2016\)](#). We describe them here briefly, for completeness. These were local shearing Cartesian box simulations of a vertically stratified distribution of ISM; performed with the NIRVANA MHD code ([Ziegler 2008](#)). The computational domain represented a patch of the galactic disk with properties consistent with those in the solar neighbourhood. Radial (x) and azimuthal (y) extent of this box was roughly 1 kpc by 1 kpc while it extended from ~ -2 to 2 kpc on either sides of galactic midplane. Shearing periodic and periodic boundary conditions were used in x and y directions, respectively, to facilitate the shear and approximate axisymmetry. While the outflow conditions were used at the upper and lower boundaries to allow for the gas outflows, but to restrict the gas inflow. A flat rotation curve was implemented by having a radially dependent angular velocity $\Omega \propto R^{-1}$, such that Ω_0 at the centre of the domain was $100 \text{ km s}^{-1} \text{ kpc}^{-1}$. Turbulence was driven by the SN explosions modelled as the local injections of thermal energy ($\sim 10^{51}$ erg per explosion) at a predefined rate of $\sim 7.5 \text{ kpc}^{-2} \text{ Myr}^{-1}$.

With this setup the mean ² magnetic field energy exponentially amplified with an e-folding time of $\sim 100 \text{ Myr}$ for a Gyr, until it reached equipartition with the turbulent kinetic energy. This growth drastically slowed down afterwards. We termed the initial exponential amplification phase (up to $\sim 1 \text{ Gyr}$) as the kinematic phase and the latter as the dynamical phase of magnetic field evolution, wherein the mean magnetic field is dynamically significant to affect the turbulent motions. Vertical profiles of the components of mean magnetic field went through several sign reversals and parity changes throughout the kinematic phase of evolution and achieved a stable mode, symmetric about the galactic mid-plane, with a strength of $\sim \mu \text{ G}$ in the mid-plane. In [Fig. 1](#) the time evolution of mean magnetic energy is shown along with the evolution of the vertical profile of y component of mean magnetic field. In [Bendre et al. \(2015\)](#) we have demonstrated that the initial exponential amplification phase of the magnetic field can be described as a solution of an α - Ω dynamo, and that the profiles of the dynamo coefficients (as measured using the test-field method) quench during the dynamical phase. Our estimates of the same system using the SVD method ([Bendre et al. 2020](#)) also agreed largely with this assertion. Therefore to have a reasonable comparison we use the data from the same model to test this new method of computing the dynamo coefficients.

3 METHODS FOR OBTAINING DYNAMO COEFFICIENTS

3.1 The IROS method

We describe here the IROS algorithm used to extract the dynamo coefficients associated with aforementioned MHD simulations. In this section, we apply it to the local representation of the EMF as given in [Eq. 1](#). [Appendix A](#) generalises it further and applies the algorithm to the non-local representation. For this analysis we first define the mean components by averaging them over the $x - y$ plane,

² Here the mean is defined as an average over the $x - y$ plane as defined in [Eq. 2](#), and it also follows the Reynold's rules mentioned in [Section 1](#)

which leaves only z as an independent variable,

$$\overline{\mathbf{F}}(z, t) = \frac{1}{L_x L_y} \iint \mathbf{F}(x, y, z, t) dx dy. \quad (2)$$

Here \mathbf{F} represents any dynamical variable \mathbf{B} , \mathbf{U} , \mathbf{J} ($\mathbf{J} = \nabla \times \mathbf{B}$) or $\overline{\mathcal{E}}$, while L_x and L_y are the sizes of the numerical domain in radial and azimuthal directions, respectively.

We then represent [Eq. 1](#) as an over-determined system of equations, by taking advantage of the fact that the dynamo coefficients do not change appreciably throughout the kinematic phase, since the mean field is not strong enough to affect the turbulence. Therefore, at any fiducial position $z = z'$ we can write

$$\mathbf{y}(z', t) = \mathbf{A}(z', t) \mathbf{x}(z'), \quad (3)$$

such that the matrices \mathbf{y} and \mathbf{A} are of dimensions $N_t \times 2$ and $N_t \times 4$ respectively and comprised of time series (t_1 to t_N) of both components of the EMF, mean magnetic fields and mean currents, and \mathbf{x} contains the dynamo coefficients. These matrices are

$$\mathbf{y}(z', t) = \begin{bmatrix} \overline{\mathcal{E}}_x(z', t_1) & \overline{\mathcal{E}}_y(z', t_1) \\ \overline{\mathcal{E}}_x(z', t_2) & \overline{\mathcal{E}}_y(z', t_2) \\ \vdots & \vdots \\ \overline{\mathcal{E}}_x(z', t_N) & \overline{\mathcal{E}}_y(z', t_N) \end{bmatrix}, \quad (4)$$

$$\mathbf{A}^\top(z', t) = \begin{bmatrix} \overline{B}_x(z', t_1) & \overline{B}_x(z', t_2) & \dots & \overline{B}_x(z', t_N) \\ \overline{B}_y(z', t_1) & \overline{B}_y(z', t_2) & \dots & \overline{B}_y(z', t_N) \\ -\overline{J}_x(z', t_1) & -\overline{J}_x(z', t_2) & \dots & -\overline{J}_x(z', t_N) \\ -\overline{J}_y(z', t_1) & -\overline{J}_y(z', t_2) & \dots & -\overline{J}_y(z', t_N) \end{bmatrix}, \quad (5)$$

and

$$\mathbf{x}(z') = \begin{bmatrix} \alpha_{xx}(z') & \alpha_{yx}(z') \\ \alpha_{xy}(z') & \alpha_{yy}(z') \\ \eta_{xx}(z') & \eta_{yx}(z') \\ \eta_{xy}(z') & \eta_{yy}(z') \end{bmatrix}. \quad (6)$$

Unlike [Eq. 1](#), this system can be solved for $\mathbf{x}(z')$ by the least-square minimisation using the IROS method described below.

3.1.1 Step 1

The IROS scheme we discuss here relies upon the incremental refinements to the estimates of dynamo coefficients. For that we first set all dynamo coefficients $\alpha_{ij}(z)$ and $\eta_{ij}(z)$ to zero. Then at any particular $z = z'$, we fit the time series of the i^{th} component of the EMF obtained from the simulations, $\overline{\mathcal{E}}_i(z', t)$ with those of $\overline{B}_x(z', t)$, $\overline{B}_y(z', t)$, $\overline{J}_x(z', t)$, and $\overline{J}_y(z', t)$, separately (i.e. by keeping only one component of \mathbf{x}_i non-zero and setting other components to zero) and obtain the zeroth level estimates ${}^0\alpha_{ix}(z')$, ${}^0\alpha_{iy}(z')$, ${}^0\eta_{ix}(z')$, and $\eta_{iy}(z')$ of dynamo coefficients along with their respective chi-squared errors ($\chi_{il}^2(z')$ with $l = 0, 1, 2, 4$). Note the superscript '0' is used to indicate the zeroth level of refinement to the EMF. The

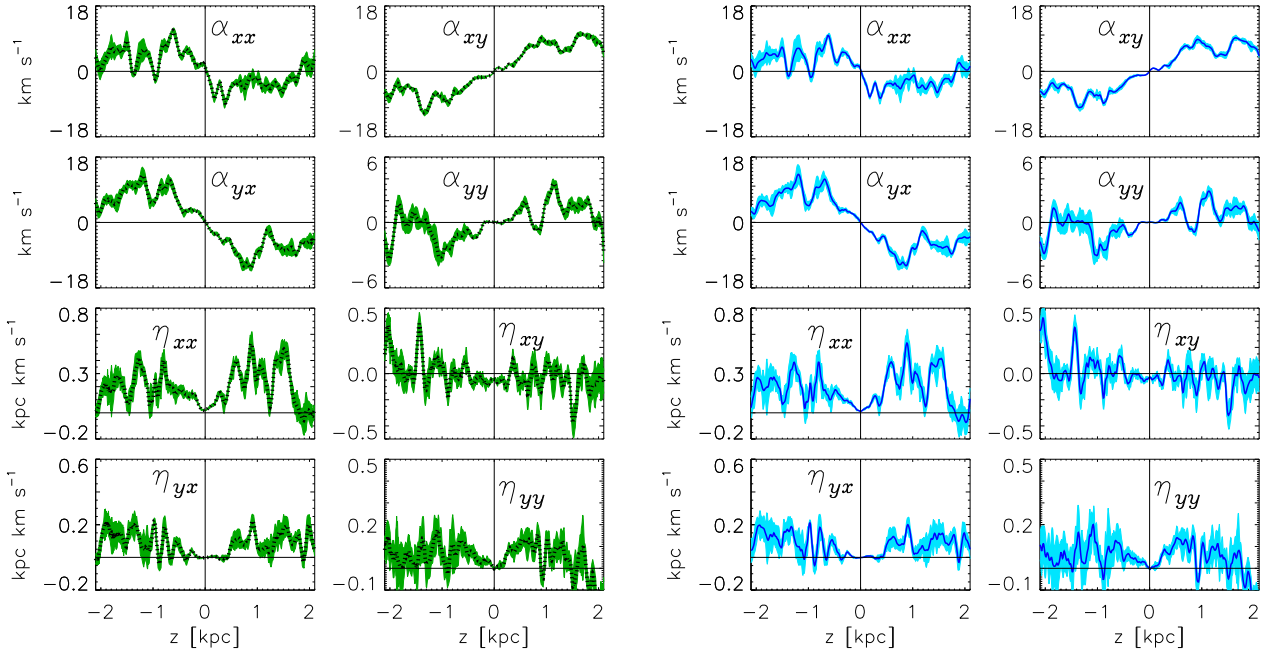


Figure 2. In left hand panels with black dotted line we show the vertical profiles of dynamo coefficients obtained by applying local SVD method to the data of MHD simulations, along with errors which are shown with green shaded region. The panels on right hand side indicate the same but the local IROS method has been used, the coefficients are shown with dark blue solid line and the respective errors are shown with regions shaded in light blue.

chi-squared errors are defined as;

$$\begin{aligned}
 \chi_{i0}^2(z') &= \sum_t \left(\bar{\mathcal{E}}_i(z', t) - {}^0\alpha_{ix}(z') \bar{B}_x(z', t) \right)^2, \\
 \chi_{i1}^2(z') &= \sum_t \left(\bar{\mathcal{E}}_i(z', t) - {}^0\alpha_{iy}(z') \bar{B}_y(z', t) \right)^2, \\
 \chi_{i2}^2(z') &= \sum_t \left(\bar{\mathcal{E}}_i(z', t) + {}^0\eta_{ix}(z') \bar{J}_x(z', t) \right)^2, \\
 \chi_{i3}^2(z') &= \sum_t \left(\bar{\mathcal{E}}_i(z', t) + {}^0\eta_{iy}(z') \bar{J}_y(z', t) \right)^2. \quad (7)
 \end{aligned}$$

3.1.2 Step 2

We then subtract from the EMF of the previous step $\bar{\mathcal{E}}_i(z', t)$, the contribution corresponding to best fitted dynamo coefficient (the one with the least of chi-square error) multiplied a suitable scale-factor $\epsilon < 1$. The factor ϵ is referred to as the “loop gain” in radio astronomy. For example, if the chi-square error associated with ${}^0\alpha_{iy}(z')$ in *Step 1* (i.e. $\chi_{i1}^2(z')$) happens to be the smallest amongst the four, we subtract the contribution $\epsilon {}^0\alpha_{iy}(z') \bar{B}_y(z', t)$ from $\bar{\mathcal{E}}_i(z', t)$ (i.e. from the EMF of the previous step) and obtain the next level of refinement to the fit of EMF, ${}^1\bar{\mathcal{E}}_i(z', t)$.

3.1.3 Step 3

Only the best fitted zeroth order estimates are retained, while the rest are set zero. For example if $\chi_{i1}^2(z')$ from *Step 2* is the smallest, only ${}^0\alpha_{iy}(z')$ is retained, while ${}^0\alpha_{ix}(z')$, ${}^0\eta_{ix}(z')$ and ${}^0\eta_{iy}(z')$ are set to zero. All dynamo coefficients are then updated by adding to them their zeroth level estimates multiplied by the loop gain.

3.1.4 Step 4

Step 1 is then repeated with ${}^1\bar{\mathcal{E}}_i(z', t)$ as the EMF to obtain ${}^1\alpha_{ix}(z')$, ${}^1\alpha_{iy}(z')$, ${}^1\eta_{ix}(z')$, and ${}^1\eta_{iy}(z')$, i.e. the first level estimates of dynamo coefficients (along with their respective chi-square errors). The estimates of dynamo coefficients are further refined by adding to them the corresponding first level contribution, which had the least chi-square error, multiplied by the loop gain ϵ . For example, if the chi-square associated with ${}^1\alpha_{ix}(z')$ happens to be the least, a factor of $\epsilon {}^1\alpha_{ix}(z')$ is added to $\alpha_{ix}(z')$. The corresponding contribution to the EMF is again subtracted after weighting by the loop gain to determine the residual ${}^2\bar{\mathcal{E}}_i$.

3.1.5 Step 5

Step 1, *Step 2* and *Step 3* are then repeated a suitable number of times (say R), until the values of the coefficients converge or all chi-squared error values drop below a certain threshold (say T). Note that the coefficient associated with the least chi-square could be different for different iterations. Effectively, the final estimates for dynamo coefficients become;

$$\alpha_{ij}(z') = \epsilon \sum_{r=0}^R r \alpha_{ij}(z') \quad (8)$$

$$\eta_{ij}(z') = \epsilon \sum_{r=0}^R r \eta_{ij}(z') \quad (9)$$

The aforementioned steps are then repeated at all $z = z'$, to construct the vertical profiles of all dynamo coefficients. A further clarification of the IROS algorithm is provided in Appendix B using a flowchart representation of aforementioned steps. We describe the vertical profiles obtained (for MHD simulations described in Section 2) using this algorithm in Section 5 below. Before that we also consider how

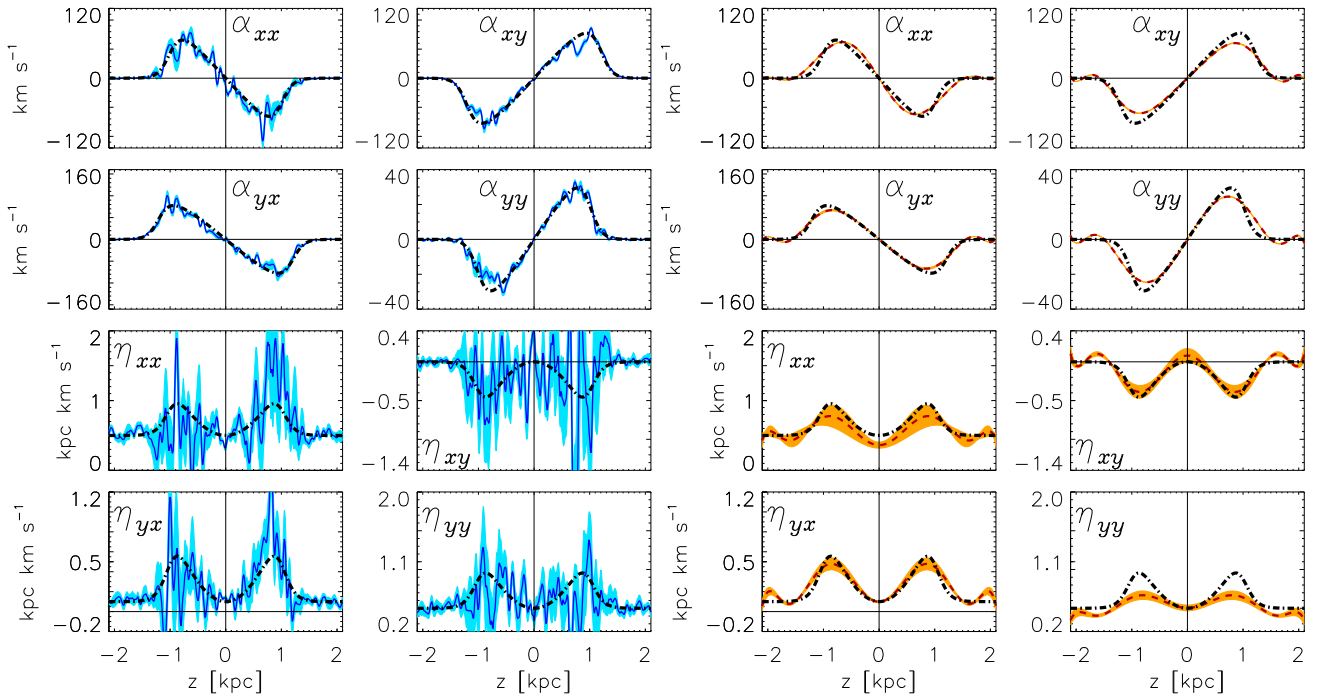


Figure 3. In the panels on the left hand side, with dark blue solid lines the vertical profiles of dynamo coefficients, computed from mock EMF data (with additive noise) using the local IROS method are shown. With light blue coloured region we have indicated the $1 - \sigma$ error intervals. The profiles shown with black dot-dashed lines indicate the dynamo coefficients used to generate the mock data. In the panels on the right hand side panels the same is shown but the red dashed lines indicate the coefficient recovered using cIROS method, and the orange colour is used to indicate the corresponding $1 - \sigma$ error.

prior constraints can be incorporated in the IROS reconstruction of dynamo coefficients.

3.2 Imposing prior constraints on the dynamo coefficients

The problem of inverting the closure for turbulent EMF can be equivalently treated in the framework of Bayesian inference by subjecting the likelihoods of the dynamo coefficients to the relevant priors. Such an approach is justified due to the helical nature of dynamo generated mean fields, which renders the components of mean fields and currents proportional to each other and thus introduces cross-correlations between dynamo coefficients (Bendre et al. 2015). In order to then be able to infer the α_{ij} and η_{ij} separately it is useful to have reasonable priors for them. Indeed, such physically informed priors on dynamo coefficients can be self consistently incorporated in the framework of IROS by putting constraints on the profiles of the coefficients, without having to invoke the Bayesian approach. This is due to the fact that the criterion for judging the best fitted parameter to the EMF at each level of refinement (for Fig. 2 and Fig. A2 it is the least of chi-squared errors of the individual fits) can be chosen so as to impose the said constraint. For example in the ISM simulations it is conceivable for coefficients α_{ij} to be anti-symmetric with respect to the galactic mid-plane, owing to the mirror asymmetry of vertically stratified helical turbulence. Similarly for η_{ij} a symmetric vertical profile can be reasonably expected due to statistical symmetry of turbulent kinetic energy on either sides of the mid-plane. Such symmetries are explicitly seen to obtain in closure calculations of the dynamo coefficients (Krause & Raedler 1980; Rädler et al. 2003; Brandenburg & Subramanian 2005; Shukurov & Subramanian 2021). Hence, a prior on dynamo coefficients can be formally incorporated in the aforementioned algorithm of IROS described in

Section 3.1, and we apply it to the same data of ISM simulations as follows. We will refer to this method as ‘constrained IROS’ or ‘cIROS’.

Firstly, we set the zeroth level dynamo coefficients $\alpha_{ij}(z)$ and $\eta_{ij}(z)$ to zero as before. Then *Step 1*, (Section 3.1.1) of the k^{th} refinement of IROS is modified as follows in cIROS: The vertical profiles of (the k^{th} order) estimates of dynamo coefficients $^k\alpha_{ij}(z)$ and $^k\eta_{ij}(z)$, (its full functional form) is first determined by again keeping each of these *functions* non zero, turn by turn, and using Eq. 1 at each time t_i . The functional form of the coefficients $^k\alpha_{ij}(z)$ are expanded in terms of Legendre polynomials of odd degrees while the $^k\eta_{ij}$ ’s are expanded using ones with even degrees, and the expansion coefficients are used to obtain the fits

$$f_k^{\alpha_{ij}}(z) = \sum_{\ell=0}^n a_{2\ell+1} P_{2\ell+1}(z/L_z), \quad (10)$$

and

$$f_k^{\eta_{ij}}(z) = \sum_{\ell=0}^n a_{2\ell} P_{2\ell}(z/L_z). \quad (11)$$

Here, a_m are the fitting parameters³, $P_m(z/L_z)$ the Legendre polynomials of degree m , and L_z , the vertical extent of the simulation domain in z direction (~ 2 kpc). Thus $f_k^{\alpha_{ij}}(z)$ is an odd function of z , while $f_k^{\eta_{ij}}(z)$ is even in z as required by our prior. The choice of n , the number of polynomials to be included in the fit, is a free parameter. Then to determine the best fitted dynamo coefficient, the

³ These parameters are determined by using the orthogonality property of Legendre polynomials

chi-square errors associated with $f_k^{\alpha_{ij}}(z)$ and $f_k^{\eta_{ij}}(z)$, denoted as χ_{il}^2 , are compared. Chi-square errors here are then defined as

$$\begin{aligned}\chi_{i0}^2 &= \sum_z \sum_t \left(\bar{\mathcal{E}}_i(z, t) - f_k^{\alpha_{ix}}(z) \bar{B}_x(z, t) \right)^2, \\ \chi_{i1}^2 &= \sum_z \sum_t \left(\bar{\mathcal{E}}_i(z, t) - f_k^{\alpha_{iy}}(z) \bar{B}_y(z, t) \right)^2, \\ \chi_{i2}^2 &= \sum_z \sum_t \left(\bar{\mathcal{E}}_i(z, t) + f_k^{\eta_{ix}}(z) \bar{J}_x(z, t) \right)^2, \\ \chi_{i3}^2 &= \sum_z \sum_t \left(\bar{\mathcal{E}}_i(z, t) + f_k^{\eta_{iy}}(z) \bar{J}_y(z, t) \right)^2.\end{aligned}\quad (12)$$

Note here, that these errors are not only summed over time but also summed over z and thus relate to the overall shape of the vertical profiles of dynamo coefficients. The determination of the best fit coefficient in cIROS is not therefore made separately at each z' , as opposed to that in previous case give in Eq. 7.

Further, in *Step 2* (Section 3.1.2) the contribution to the EMF associated with the least chi-squared weighted with the loop-gain factor (that is, either $\epsilon f_k^{\alpha_{ij}} \bar{B}_j$ or $-\epsilon f_k^{\eta_{ij}} \bar{J}_j$) is subtracted from $\bar{\mathcal{E}}_i$. *Step 3*, *step 4* and *5* are then performed the same way as described in Section 3.1.3, Section 3.1.4 and Section 3.1.5. Fitting at each z is now not necessary as the z dependence of the coefficients is already taken into account in the polynomial fit. The resulting vertical profiles of the dynamo coefficient are

$$\alpha_{ij}(z) = \epsilon \sum_{r=0}^R f_r^{\alpha_{ij}}(z), \quad (13)$$

$$\eta_{ij}(z) = \epsilon \sum_{r=0}^R f_r^{\eta_{ij}}(z). \quad (14)$$

We discuss the results of this analysis and compare the performance of cIROS on the determination of dynamo coefficients in Section 5.2. Additionally we test these two methods against the mock data of a noisy EMF in the following Section 4.

4 TESTING THE IROS METHOD USING MOCK DATA

We test the ability of the regular and the constrained IROS method to correctly estimate the profiles of dynamo coefficients by treating with it the mock data of the EMF generated from the mean magnetic fields. For this purpose we first prescribe the vertical profiles of mock dynamo coefficients $\alpha_{ij}^m(z)$ and $\eta_{ij}^m(z)$, which are shown with black dot-dashed lines in Fig. 3, and use the time evolution data of the vertical profiles of mean fields and currents ($\bar{\mathbf{B}}(z, t)$ and $\bar{\mathbf{J}}(z, t)$) from the ISM simulations (discussed in Section 2) to construct also the $z-t$ profiles of EMF using Eq. 1. Furthermore to construct mock data of the noisy EMF $\bar{\mathcal{E}}^m(z, t)$, a uniform random distribution of noise of increasing power is added on the top of it, such that the local ratios of noise to signal range from 10% to 300%. We note here also that the contribution of $\alpha_{ij}^m(z)$ to the $\bar{\mathcal{E}}^m(z, t)$ is taken to be much larger compared to that from $\eta_{ij}^m(z)$. This is to ensure the efficacy of IROS to still determine the rest of the coefficients in situation where only few coefficients contribute overwhelmingly to the EMF. (Thus our mock data test is much more stringent than that required by the actual data).

We find that the IROS method in its unmodified version can determine most dynamo coefficients with accuracy up to the noise level of $\sim 50\%$, and loses its efficacy to determine especially the η_{ij}

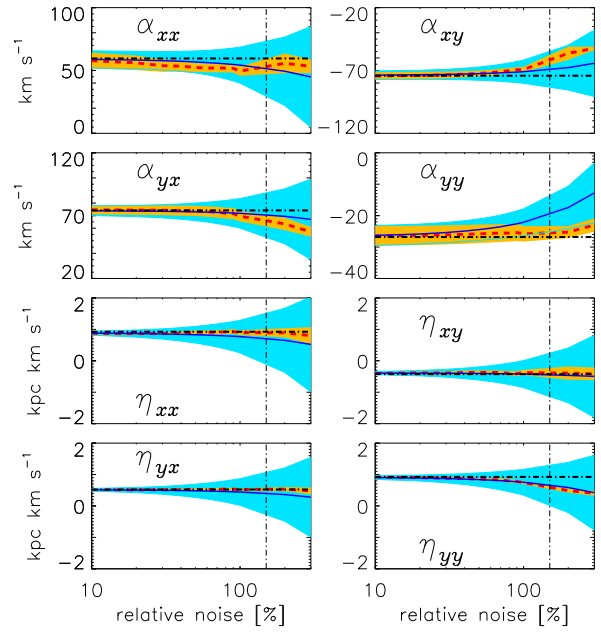


Figure 4. Plotted in dark blue-solid line style are the estimates of the dynamo coefficients, averaged between $z = -1$ kpc to -0.7 kpc, as functions of imposed error on the EMF, calculated with the IROS method. The associated variance shown with light blue colour. With the red dashed line we plot the dynamo coefficients averaged over the same z domain, but estimated using the cIROS method along with the corresponding variance shown in orange. The black dot-dashed line are the imposed dynamo coefficients that make the mock EMF data. The vertical dot-dashed line corresponds to the 150% of added noise to the mock EMF, to which Fig. 3 corresponds.

beyond the noise level of $\sim 50\%$, whereas with the constrained IROS or cIROS the coefficients can be determined reasonably up to a noise level of $\sim 200\%$. This is demonstrated in Fig. 4 where we can see that errors (shown in colour light blue) in the determinations of η_{ij} with the regular IROS are overwhelmingly large beyond the noise level of $\sim 50\%$. While with cIROS method they are well constrained, as shown with the colour orange.

We want to clarify here the reason for using the mean-field data from the direct MHD simulations to construct the mock data of EMF, rather than one realised in the one dimensional dynamo simulations. The components of mean-field produced in pure $\alpha - \Omega$ dynamo simulations are completely correlated, and it is difficult to determine the associated dynamo coefficients separately, with any least-square minimisation method including IROS. Another source of error in determining dynamo coefficients from the data of direct simulations is additive noise in the EMF, which can however be handled with these methods.

5 RESULTS

5.1 IROS inversion using the local EMF representation

We apply the method discussed in Section 3.1 to the data of MHD simulations of ISM described in Section 2, and obtain the associated dynamo coefficients. We first extract the time series of the EMF, mean-fields and mean currents from the simulations and split them in nine different sections by successively skipping eight points. For each of these realisations we obtain all dynamo coefficients, using the aforementioned IROS method. In right hand panel of Fig. 2

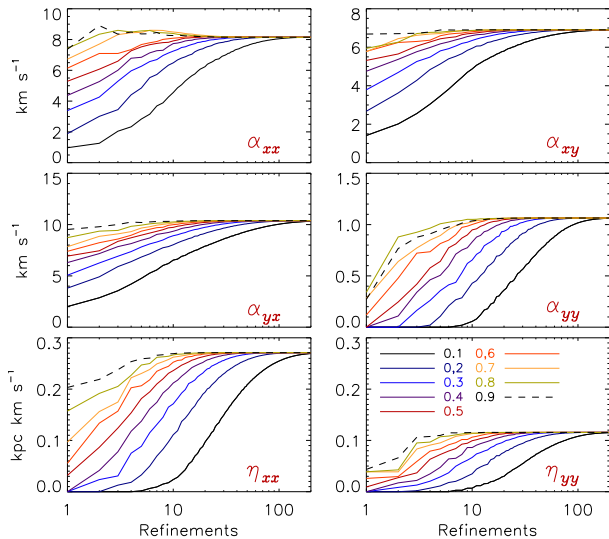


Figure 5. The obtained values of the dynamo coefficients as a function of the number of refinements. Shown in different colours are different loop gains ϵ (10% to 90%); see the colour code in the lower right panel. Dynamo coefficients are calculated at a specific height (~ 700 pc), using the local version of IROS.

with dark blue solid lines we have shown the average of these nine outcomes, along with associated errors using light blue shades, which are obtained from the variance in these nine results. Here we have used the loop gain ϵ of 0.3 and a hundred levels of refinements in total ($R = 100$). Additionally these simulations have already been analysed using local SVD method. In the left hand panels of the same figure we plot the estimates of dynamo coefficients obtained using SVD with black dotted lines, along with their respective errors obtained in the same way by a green shade. It can be seen that both these methods give very similar results although employing very different algorithms in detail.

We also perform the same exercise for different values of ϵ and track the values of refined dynamo coefficients as a function of refinements. It appears that as we refine these coefficients in IROS, they converge to their true values logarithmically. The rate of convergence is unsurprisingly faster for the larger values of loop gain ϵ . We demonstrate this in Fig. 5, for the local version of IROS method, where we plot the magnitudes of various dynamo coefficients at ~ 800 pc, as functions of refinements, with different line styles indicating the various loop gains as indicated in the lower-right hand panel.

5.2 cIROS inversions using prior constraints

In a similar way we use the constrained IROS method (Section 3.2) to invert the local $\bar{\mathcal{E}}$ representation. We use the same ISM simulations data discussed in Section 2 and using $n = 40$ even and odd Legendre polynomials to fit the dynamo coefficients during each cIROS iteration, and obtain their vertical profiles. These are shown in Fig. 6. With red dashed lines we show the profiles obtained with the constrained IROS method along their errors shown in the orange shaded region. While with the blue solid lines we show the same with the unconstrained IROS method described in Section 3.1. We see that these two methods of inversions give qualitatively similar results, although the α_{ij} and η_{ij} coefficients determined using cIROS after imposing priors are firstly antisymmetric and symmetric respectively, with re-

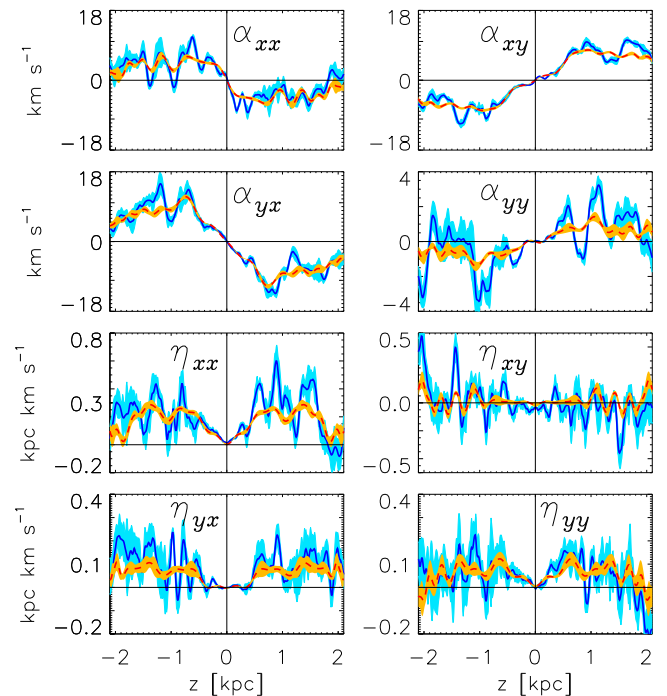


Figure 6. Shown with red dashed lines are the vertical profiles of dynamo coefficients computed using the cIROS method. Associated errors are shown with orange shaded regions. While the dark blue solid lines show the dynamo coefficient profiles computed with the IROS method (same as in the left hand panels of Fig. 2), along with their associated errors are shown with light blue shaded regions.

spect to the midplane, and secondly their profiles are smoother with smaller errors.

Even without applying these constraints, the rough tendencies of even or odd parities of the vertical profiles of the most coefficients can already be seen in the results of IROS (and SVD) methods Fig. 5, which is to be expected for the SN driven ISM turbulence. We note here, however, that the priors used for α_{ij} and η_{ij} are specific to the ISM simulations where the parities of the coefficients can be inferred from underlying physics. These need not be valid for other astrophysical systems. However any other physically informed constraint specific to a particular system or more general priors can be similarly incorporated in the framework of IROS.

6 CONCLUSIONS

Estimation of the dynamo coefficients associated with MHD simulations is crucial in understanding the large-scale dynamo effect as well as in quantifying the connection of MHD turbulence to the evolution of large-scale magnetic fields. This is usually accomplished using either the test-field method, which requires multiple additional induction equations to be solved along with the DNS, or using the post-processing methods based on regression which tend to be relatively faster. The SVD method for example directly solves Eq. 1 in post-processing, by assuming the constancy of dynamo coefficients in time and inverting Eq. 3 instead. Problems associated with directly inverting Eq. 1, usually stem from having a statistical correlation between $\bar{\mathbf{B}}$ and $\bar{\mathbf{J}}$ (for example in α^2 -dynamoes, $\bar{\mathbf{J}} \sim \nabla \times \bar{\mathbf{B}} - k \bar{\mathbf{B}}$, which further introduces correlations in α_{ij} and η_{ij}), or having one

(or more) of the components of $\bar{\mathbf{B}}$ or $\bar{\mathbf{J}}$ contribute overwhelmingly to the EMF. The latter issue in particular leads to the underestimation of the dynamo coefficients associated with the components of the mean field or current that contribute negligibly to the EMF or are comparatively noisier.

In this paper we present a new post processing tool, IROS, which mitigates this later problem, apart from having a number of other advantages. In IROS the components of EMF are successively fit against the individual mean field and current components, and the estimates of dynamo coefficients obtained in the fits are refined iteratively by removing the contribution of the best fitted parameters from the EMF, thus circumventing the aforementioned issue. Following a similar algorithm we further extended this method to also invert the non-local representation of EMF to determine the components of the non-local kernel \mathcal{K}_{ij} , as described in Appendix A. Significantly, we also show that it is possible in IROS to impose reasonable prior constraints on the dynamo coefficients. This constrained IROS method (“cIROS”), makes an appropriate modification to the criterion of the best fit at each iteration of the IROS refinement. As an example, we impose the priors on the vertical profiles of dynamo coefficients, such that $\alpha_{ij}(z)$ and $\eta_{ij}(z)$ with respect to the mid-plane ($z = 0$) are antisymmetric and symmetric respectively. This was done simply by expanding the dynamo coefficient profiles in terms of either odd or even Legendre polynomials and modifying the definitions of chi-squared errors to measure the goodness of the EMF fit with respect to these Legendre expansions, as described in Section 3.2. We note here that a different set of prior constraints specific to the system can be incorporated in the same way with appropriate definitions of chi-squared errors. Moreover a probabilistic framework can also be adopted to impose the said priors, self consistently.

To have a reasonable validation of the IROS method we applied it to the data of ISM simulations, which has been analysed before using the test-field method as well as the local and non-local variants of the SVD method. The vertical profiles of the dynamo coefficients recovered from the IROS and the SVD method are found to be largely consistent with each other (as shown in Fig. 2 and Fig. A2). We also applied this method to the synthetic data with predefined vertical profiles of dynamo coefficients chosen such that only a few of the coefficients contributed largely to the EMF, and with varying levels of additive noise. We demonstrated that even with the noise level as high as 200% of the EMF, using IROS we were still able to recover the dynamo coefficients with a reasonable accuracy, and considerably better than the SVD method. We have applied these methods to compute the dynamo coefficients associated with other simulations, with a reasonable degree of success. For example in (Dhang et al. 2023) we apply these methods for the local simulations of accretion disc, where the turbulence is driven by the magnetorotational instability. While in (Qazi et al. 2024) we use them in the simulations where the turbulence is driven by the magnetic buoyancy instability.

With this analysis we have shown that the IROS method could serve as a viable method to determine the dynamo coefficients. As a post-processing tool, it firstly has an advantage of being extremely computationally efficient compared to the test-field method, while also being more robust in handling the additive noise than the SVD. A conceivable disadvantage in the standard IROS (and also in the SVD), however, is that the determined dynamo coefficients get correlated when the components of mean-field and current are correlated as well. This is avoided in the test-fields method since the additional linearly independent test magnetic fields are also evolved along with the MHD simulations. In this respect, it is useful to have a possibility, as in the cIROS, of imposing prior constraints on dynamo coefficients to break the degeneracy between α_{ij} and η_{ij} . It would also be useful

to extend the the cIROS to invert the integral or kernel representation of EMF and to impose prior constraints on the coefficients of the non-local kernel.

ACKNOWLEDGEMENTS

We thank Dipankar Bhattacharya for valuable insights and for a detailed tutorial on IROS. We also thank Neeraj Gupta, Maarit J. Korpi-Lagg, and Matthias Rheinhardt for their valuable insights and explanations. J.S. and A.B. acknowledge the support by the Swiss National Science Foundation under Grant No. 185863.

DATA AVAILABILITY

The data underlying this article will be shared on reasonable request to the corresponding author.

REFERENCES

- Beck R., Wielebinski R., 2013, *Magnetic Fields in Galaxies*. Springer Berlin Heidelberg, p. 641, doi:10.1007/978-94-007-5612-0_13
- Bendre A. B., 2016, doctoralthesis, Universität Potsdam
- Bendre A. B., Subramanian K., 2022, *MNRAS*, 511, 4454
- Bendre A., Gressel O., Elstner D., 2015, *Astronomische Nachrichten*, 336, 991
- Bendre A. B., Subramanian K., Elstner D., Gressel O., 2020, *MNRAS*, 491, 3870
- Brandenburg A., 2005, *Astronomische Nachrichten*, 326, 787
- Brandenburg A., 2009, *Space Science Reviews*, 144, 87
- Brandenburg A., 2018, *Journal of Plasma Physics*, 84, 735840404
- Brandenburg A., Sokoloff D., 2002, *Geophysical & Astrophysical Fluid Dynamics*, 96, 319
- Brandenburg A., Subramanian K., 2005, *Physics Reports*, 417, 1
- Cattaneo F., Hughes D. W., 1996, *Physical Review E*, 54, 4532
- Dhang P., Bendre A., Sharma P., Subramanian K., 2020, *MNRAS*, 494, 4854
- Dhang P., Bendre A., Subramanian K., 2023, *arXiv e-prints*, p. arXiv:2308.07959
- Gressel O., Pessah M. E., 2015, *ApJ*, 810, 59
- Gressel O., Elstner D., Ziegler U., Rüdiger G., 2008, *Astronomy and Astrophysics*, 486, L35
- Hammersley A., Ponman T., Skinner G., 1992, *Nuclear Instruments and Methods in Physics Research A*, 311, 585
- Högbom J. A., 1974, *A&AS*, 15, 417
- Käpylä P. J., Korpi M. J., Brandenburg A., 2009, *Astronomy and Astrophysics*, 500, 633
- Kowal G., Otmianowska-Mazur K., Hanasz M., 2006, *A&A*, 445, 915
- Krause F., Rädler K. H., 1980, *Mean-field magnetohydrodynamics and dynamo theory*. Pergamon Press
- Moffatt H. K., 1978, *Magnetic Field Generation in Electrically Conducting Fluids*. Cambridge University Press, Cambridge
- Park K., Cheoun M. K., Kim C.-B., 2023, *The Astrophysical Journal*, 944, 2
- Qazi Y., Shukurov A., Tharakkal D., Gent F. A., Bendre A. B., 2024, *MNRAS*, 527, 7994
- Racine É., Charbonneau P., Ghizaru M., Bouchat A., Smolarkiewicz P. K., 2011, *The Astrophysical Journal*, 735, 46
- Rädler K.-H., Kleeorin N., Rogachevskii I., 2003, *Geophysical and Astrophysical Fluid Dynamics*, 97, 249
- Rüdiger G., Hollerbach R., 2004, *The magnetic universe : geophysical and astrophysical dynamo theory*. Wiley-VCH
- Schrinner M., Rädler K.-H., Schmitt D., Rheinhardt M., Christensen U., 2005, *Astronomische Nachrichten*, 326, 245
- Schrinner M., Rädler K.-H., Schmitt D., Rheinhardt M., Christensen U. R., 2007, *Geophysical and Astrophysical Fluid Dynamics*, 101, 81

- Shukurov A., Subramanian K., 2021, *Astrophysical Magnetic Fields: From Galaxies to the Early Universe*. Cambridge Astrophysics, Cambridge University Press, doi:10.1017/9781139046657
- Simard C., Charbonneau P., Dubé C., 2016, *Advances in Space Research*, 58, 1522
- Sur S., Subramanian K., Brandenburg A., 2007, *Monthly Notices of the Royal Astronomical Society*, 376, 1238
- Tobias S. M., Cattaneo F., 2013, *Journal of Fluid Mechanics*, 717, 347
- Warnecke J., Rheinhardt M., Tuomisto S., Käpylä P. J., Käpylä M. J., Brandenburg A., 2016, preprint, (arXiv:1601.03730)
- Ziegler U., 2008, *Computer Physics Communications*, 179, 227

APPENDIX A: NON-LOCAL IROS METHOD

The turbulent EMF at any particular $z = z'$ can equivalently be expressed as a linear function of mean field components in its local ζ neighbourhood, through a non-local kernel \mathcal{K}_{ij} as follows.

$$\overline{\mathcal{E}}_i(z') = \int_{-\infty}^{\infty} \mathcal{K}_{ij}(z, \zeta) \overline{B}_j(z - \zeta) d\zeta. \quad (\text{A1})$$

This representation of EMF allows one to express the regular dynamo coefficients α_{ij} , η_{ij} as the zeroth and first moments of \mathcal{K}_{ij} respectively. Additionally, from the numerical perspective it has an advantage of not being dependent directly on the coefficients of current, avoiding any errors in fitting that may enter in the computation by having to numerically differentiate \mathbf{B} . Furthermore, it also accounts for the non-local contribution of mean-fields to the turbulent EMF. In (Bendre & Subramanian 2022), by varying the width of the local window, we have established that the non-local contributions up to ~ 50 pc contribute significantly to the EMF.

To express Eq. A1 in a form that can be solved by least square minimisation, we represent it first in a summation form,

$$\overline{\mathcal{E}}_i = \sum_{l=-m}^m \mathcal{K}_{ij}(z', \zeta_l) \overline{B}_j(z' - \zeta_l) \delta, \quad (\text{A2})$$

where the δ is the size of grid, and the limit l represent the number of points we want to consider in the local neighbourhood of z' . \mathcal{K}_{ij} , typically vanish as ζ_l approaches the correlation scale of turbulence, which can be determined empirically by considering various values of l . In this particular example $l = 6$ spans the local neighbourhood of z' as $6\delta (\sim 50 \text{ pc})$ approximately corresponds to the scale-length of SN driving.

We rewrite Eq. A2 then in a matrix form (similar to Eq. 3) as follows,

$$\mathbf{y}_i(z', t) = \mathbf{A}(z') \mathbf{x}_i(z', \zeta_l), \quad (\text{A3})$$

where, \mathbf{A} is a $N \times 2(2l + 1)$ matrix, comprised of \overline{B}_x and \overline{B}_y in the local neighbourhood of $z = z'$, with ζ_l being the neighbourhood variable, and $\mathbf{x}_i(z', \zeta)$ the kernel coefficients, while the $\mathbf{y}_i(z', t)$ is the column vector with EMF (component i) time series at $z = z'$. Specifically,

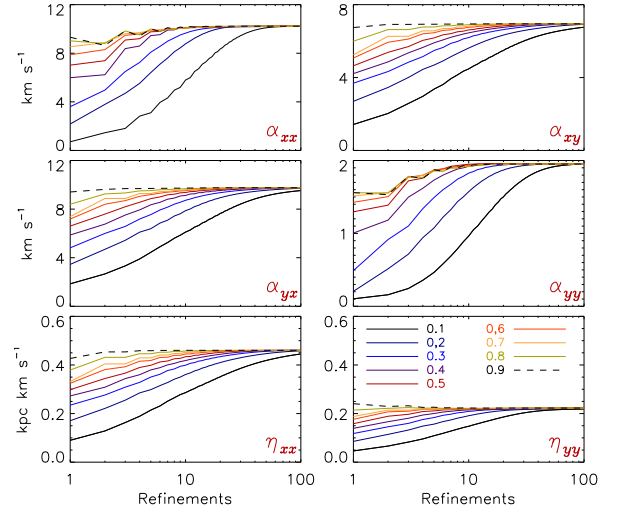


Figure A1. Same as Fig. 5 but for the dynamo coefficients computed with the non-local version of IROS.

$$\mathbf{y}_i(z', t) = \begin{bmatrix} \overline{\mathcal{E}}_i(z', t_1) \\ \overline{\mathcal{E}}_i(z', t_2) \\ \vdots \\ \overline{\mathcal{E}}_i(z', t_N) \end{bmatrix}, \quad (\text{A4})$$

$$\mathbf{x}_i(z', \zeta_l) = \begin{bmatrix} \mathcal{K}_{ix}(z' - l\delta) \\ \vdots \\ \mathcal{K}_{ix}(z' + l\delta) \\ \mathcal{K}_{iy}(z' - l\delta) \\ \vdots \\ \mathcal{K}_{iy}(z' + l\delta) \end{bmatrix}, \quad (\text{A5})$$

$$\mathbf{A}^\top(z') = \begin{bmatrix} \overline{B}_x(z' - l\delta, t_1) & \overline{B}_x(z' - l\delta, t_2) & \dots & \overline{B}_x(z' - l\delta, t_N) \\ \vdots & \vdots & & \vdots \\ \overline{B}_x(z' + l\delta, t_1) & \overline{B}_x(z' + l\delta, t_2) & \dots & \overline{B}_x(z' + l\delta, t_N) \\ \overline{B}_y(z' - l\delta, t_1) & \overline{B}_y(z' - l\delta, t_2) & \dots & \overline{B}_y(z' - l\delta, t_N) \\ \vdots & \vdots & & \vdots \\ \overline{B}_y(z' + l\delta, t_1) & \overline{B}_y(z' + l\delta, t_2) & \dots & \overline{B}_y(z' + l\delta, t_N) \end{bmatrix} \quad (\text{A6})$$

\mathcal{K}_{ij} components in this formulation relate to the regular dynamo coefficients α_{ij} and η_{ij} through following relations (see e.g. Bendre & Subramanian 2022),

$$\alpha_{ij}(z) = \int_{\zeta_l} \mathcal{K}_{ij}(z, \zeta_l) d\zeta_l$$

$$\begin{bmatrix} \eta_{xx} & \eta_{xy} \\ \eta_{yx} & \eta_{yy} \end{bmatrix} (z) = \int_{\zeta_l} \begin{bmatrix} -\mathcal{K}_{xy}(z, \zeta_l) & \mathcal{K}_{xx}(z, \zeta_l) \\ -\mathcal{K}_{yy}(z, \zeta_l) & \mathcal{K}_{yx}(z, \zeta_l) \end{bmatrix} \zeta_l d\zeta_l \quad (\text{A7})$$

To obtain then the \mathbf{x}_i such that it minimises the residual $\mathcal{R} = (\mathbf{y}_i - \mathbf{A}\mathbf{x}_i)^2$, we follow the same IROS algorithm described in Section 3.1. With a slight modification described as follows. In *Step 1* we set all the coefficients of kernel \mathcal{K}_{ij} to zero. Then, at any particular

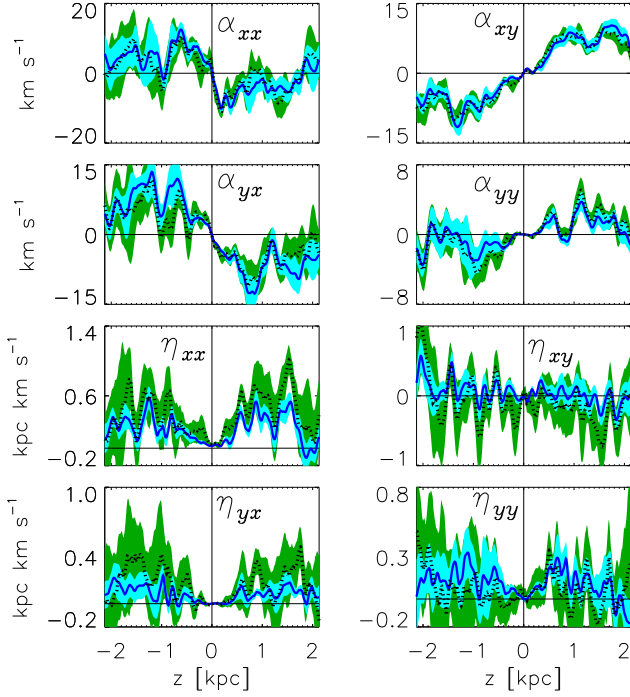


Figure A2. Same as Fig. 2 except the coefficients here are computed by applying IROS algorithm to the non-local prescription of EMF. With dark blue solid line we show the profiles of the coefficients computed using IROS method with non-local EMF prescription. The associated $1 - \sigma$ errors are shown with light blue regions. These coefficients are also comparable with once calculated using non-local SVD method shown here with black dotted lines and associated errors in light green shades. Size of the local neighbourhood considered here ranges from ~ -60 to $+60$ pc about any particular z .

$z = z'$, we fit the time series $\mathcal{E}_i(z', t)$ separately against $\bar{B}_x(z' - \zeta)$ and $\bar{B}_y(z' - \zeta)$ in the entire local ζ neighbourhood. That is, we fit $\mathbf{y}_i(z', t)$ against $\mathbf{A}^x(z')$ and $\mathbf{A}^y(z')$ separately, which contain the first and later $(2l + 1)$ columns of \mathbf{A} ,

$$\mathbf{A}^i(z') = \begin{bmatrix} \bar{B}_i(z' - l\delta, t_1) & \bar{B}_i(z' + l\delta, t_1) \\ \vdots & \vdots \\ \bar{B}_i(z' - l\delta, t_N) & \bar{B}_i(z' + l\delta, t_N) \end{bmatrix}, \quad (\text{A8})$$

and obtain ${}^0\mathcal{K}_{ix}(z', \zeta)$ and ${}^0\mathcal{K}_{iy}(z', \zeta)$, the zeroth level estimates of kernel coefficients. Consequently the definition of the chi-square errors is modified as

$$\chi_{i0}^2(z') = \sum_t \left(\mathcal{E}_i(z') - \sum_{j=-m}^m {}^0\mathcal{K}_{ix}(z', j\delta) \bar{B}_x(z' - j\delta) \right)^2, \quad (\text{A9})$$

$$\chi_{i1}^2(z') = \sum_t \left(\mathcal{E}_i(z') - \sum_{j=-m}^m {}^0\mathcal{K}_{iy}(z', j\delta) \bar{B}_y(z' - j\delta) \right)^2. \quad (\text{A10})$$

Further steps are carried out the same way described in Section 3.1, and final estimate of kernel are obtained iteratively. The results of this analysis will also be discussed in Section 5.

A1 IROS inversions using the non-local EMF representation

We now apply the method discussed in Section A to the same data. Vertical profiles of the zeroth and first moments of the dynamo coefficients (i.e. $\alpha_{ij}(z)$ and $\eta_{ij}(z)$ respectively) are shown with dark blue

solid lines in Fig. A2, along with $1 - \sigma$ error intervals shown with light blue colour shades. Value of the loop gain ϵ and refinements used for the calculation are 0.3 and one hundred respectively. These profiles seem to compare well with the estimates of the same quantities made using non-local SVD method, shown with black dotted lines along with associated errors in green coloured shade. It can be seen by comparing the error bars in this figure, that the non-local IROS performs somewhat better than the non-local SVD method. The sensitivity of the results to a change in ϵ and the number of refinements is again tested and the results shown in Fig. A1.

APPENDIX B: FLOWCHART OF THE IROS METHOD

To further clarify the local IROS algorithm discussed in Section 3.1 it can equivalently be represented as a flowchart. For example, Fig. B1 we show the flowchart of the local IROS method to determine the dynamo coefficients at $z = z'$. To similarly represent the cIROS algorithm as a flowchart, a few modifications are made. Namely, instead of reading the data y and A_k at a particular $z = z'$ the entire z profiles are read in, and after the line fitting procedure, the slopes m_{xki} are expanded in terms of Legendre polynomials to calculate the chi-squared errors using Eq. 12.

This paper has been typeset from a \LaTeX file prepared by the author.

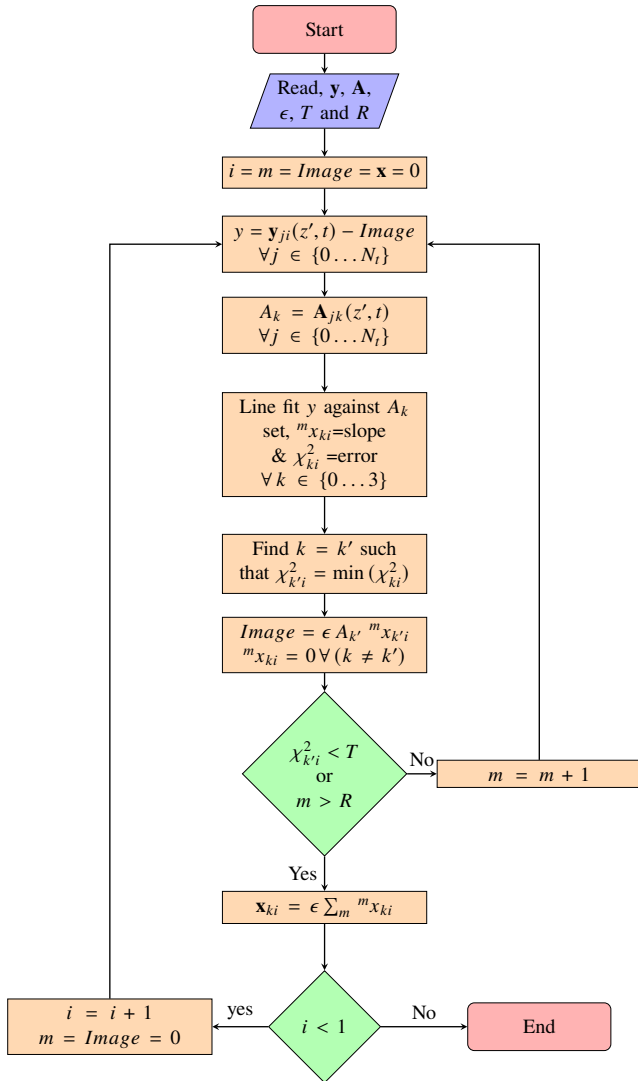


Figure B1. Flow chart representation of the local IROS algorithm.